

Circulation Research

JOURNAL OF THE AMERICAN HEART ASSOCIATION

American Heart
Association® 
*Learn and Live*SM

Contribution of IKr to Rate-Dependent Action Potential Dynamics in Canine Endocardium

Fei Hua and Robert F. Gilmour, Jr

Circ. Res. 2004;94;810-819; originally published online Feb 12, 2004;

DOI: 10.1161/01.RES.0000121102.24277.89

Circulation Research is published by the American Heart Association, 7272 Greenville Avenue, Dallas, TX 75214

Copyright © 2004 American Heart Association. All rights reserved. Print ISSN: 0009-7330. Online ISSN: 1524-4571

The online version of this article, along with updated information and services, is located on the World Wide Web at:

<http://circres.ahajournals.org/cgi/content/full/94/6/810>

Subscriptions: Information about subscribing to Circulation Research is online at
<http://circres.ahajournals.org/subscriptions/>

Permissions: Permissions & Rights Desk, Lippincott Williams & Wilkins, a division of Wolters Kluwer Health, 351 West Camden Street, Baltimore, MD 21202-2436. Phone: 410-528-4050. Fax: 410-528-8550. E-mail:
journalpermissions@lww.com

Reprints: Information about reprints can be found online at
<http://www.lww.com/reprints>

Contribution of I_{Kr} to Rate-Dependent Action Potential Dynamics in Canine Endocardium

Fei Hua, Robert F. Gilmour, Jr

Abstract—Previous modeling studies have suggested that the rapid component of the delayed rectifier (I_{Kr}) may contribute importantly to action potential dynamics during tachycardia. To test this idea experimentally, I_{Kr} was measured as the E-4031-sensitive current in isolated canine endocardial myocytes at 37°C using the perforated patch-clamp technique. Command potentials were trains of action potential waveforms recorded at cycle lengths (CLs) of 1000, 500, 320, 170, and 120 ms. Action potential duration (APD) alternans occurred at CLs of 170 and 120 ms. During an action potential, I_{Kr} increased gradually to a maximum at -55 to -60 mV. Peak I_{Kr} increased initially as CL was shortened from 1000 to 500 ms (from 0.55 ± 0.03 to 0.57 ± 0.03 pA/pF), but decreased progressively as CL was shortened further (to 0.45 ± 0.03 pA/pF at CL=120 ms). Baseline I_{Kr} was negligible at CLs of 1000 to 320 ms, but increased to 0.12 ± 0.01 pA/pF at a CL of 120 ms. During APD alternans, peak I_{Kr} was larger for the short than for the long action potential (0.48 ± 0.03 versus 0.46 ± 0.03 pA/pF). A computer model of I_{Kr} based on these data indicated that increasing I_{Kr} suppressed alternans and decreasing I_{Kr} increased alternans. In support of the latter result, inhibition of I_{Kr} by E-4031 increased the maximal amplitude of alternans. These results indicate that I_{Kr} contributes importantly to rate-related alterations of repolarization, including APD alternans. Modifying I_{Kr} may be a promising approach to suppressing alternans and thereby preventing ventricular tachyarrhythmias. (*Circ Res.* 2004;94:810-819.)

Key Words: I_{Kr} ■ alternans ■ ventricular arrhythmias

The duration of the canine ventricular action potential (APD) decreases as the pacing cycle length (CL) decreases, until at short CL, APD alternans occurs.^{1,2} The rate-dependency of APD is represented by the APD restitution relation, which is the relationship between APD and the preceding diastolic interval. Previous studies have indicated that rate-dependent APD alterations are important determinants of ventricular arrhythmias and that reducing the slope of the APD restitution relation can be antiarrhythmic.³⁻⁸ However, the available options for altering APD restitution are limited, in part because the ionic mechanism for the rate-dependency of APD is not well understood.

Several lines of evidence suggest that the L-type Ca^{2+} current (I_{Ca}) plays an important role in APD restitution and in the development of APD alternans.⁹⁻¹¹ In particular, blockade of I_{Ca} in a computer model and experimentally has been shown to reduce the slope of the APD restitution relation and to suppress ventricular fibrillation.^{4,10} The obvious drawback to this approach is that blockade of I_{Ca} also suppresses contractility. However, if reducing inward plateau current flattens the slope of the APD restitution relation, then perhaps increasing outward repolarizing current might have a similar effect. This idea has been supported by computer simula-

tions,¹⁰ but there is little experimental data regarding the role of repolarizing currents in APD restitution. Consequently in this study, we examined the possible role of the rapid component of the delayed rectifier (I_{Kr}) in rate-dependent APD alterations, including APD alternans.

I_{Kr} plays an important role in defining ventricular repolarization, as reflected by the fact that a wide variety of drugs that inhibit I_{Kr} prolong APD and the QT interval.¹²⁻¹⁶ In addition, mutation of the gene encoding I_{Kr} (HERG) underlies one form of the long-QT syndrome.^{17,18} The contribution of I_{Kr} to action potential repolarization is complex, in that during an action potential, I_{Kr} initially activates at positive membrane potentials, but then rapidly inactivates during the plateau phase. As the membrane potential repolarizes, I_{Kr} recovers from inactivation before it deactivates. As a result, I_{Kr} increases to a maximum during phase 3 of the action potential and then decreases, as the electrical driving force decreases and as deactivation of the channel increases.

Given the complex interactions between voltage, time, and magnitude of I_{Kr} , measurements of I_{Kr} during an action potential waveform may more faithfully represent the contribution of I_{Kr} to repolarization than measurements obtained from standard voltage clamp techniques. Therefore in this

Original received February 28, 2003; resubmission received October 15, 2003; revised resubmission received January 5, 2004; accepted January 29, 2004.

From the Department of Biomedical Sciences, Cornell University, Ithaca, NY.

This manuscript was sent to Michael R. Rosen, Consulting Editor, for review by expert referees, editorial decision, and final disposition.

Correspondence to Robert F. Gilmour, Jr, Department of Biomedical Sciences, T7 012 VRT, Cornell University, Ithaca, NY 14853-6401. E-mail rfg2@cornell.edu

© 2004 American Heart Association, Inc.

Circulation Research is available at <http://www.circresaha.org>

DOI: 10.1161/01.RES.0000121102.24277.89

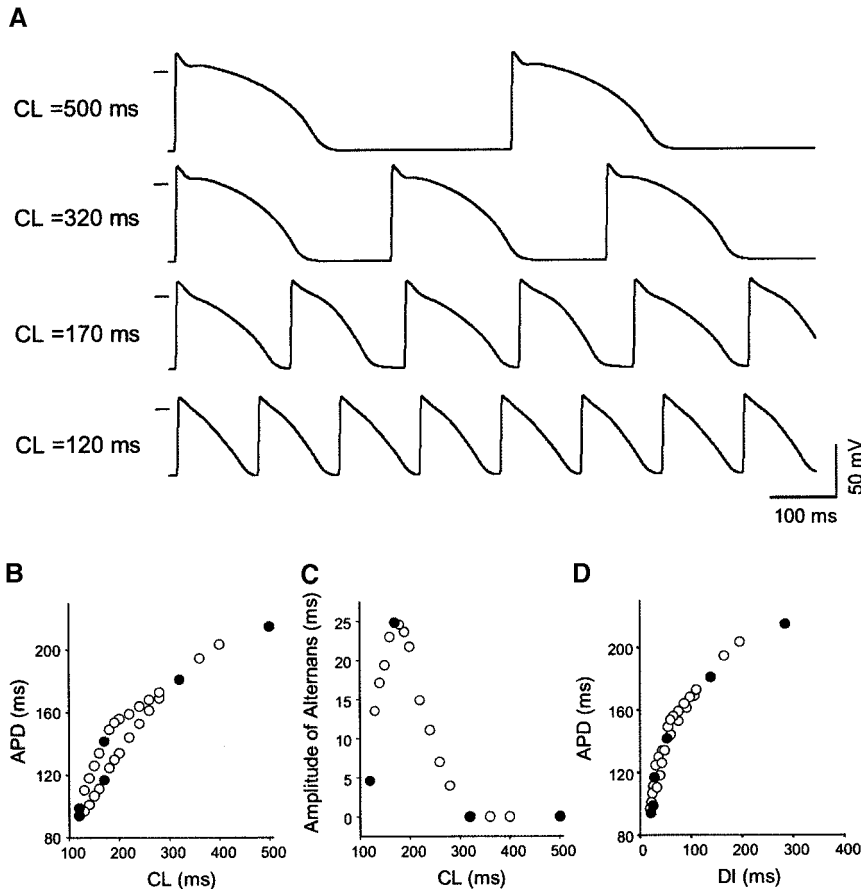


Figure 1. Selected action potentials used as waveforms for the action potential clamp. A, Action potentials at CL=500, 320, 170, and 120 ms. Black bars indicate 0 mV. B, Relationship between APD and CL. C, Relationship between the amplitude of alternans and CL. D, Relationship between APD and preceding diastolic interval (DI). Filled circles represent the CLs chosen for the patch-clamp studies.

study, the possible contribution of I_{Kr} to rate-dependent alterations of APD was assessed by measuring I_{Kr} during action potentials elicited by different pacing CLs using the action potential clamp technique. Data generated by these experiments subsequently were used to construct a computer model of I_{Kr} , which was then used to test whether increasing I_{Kr} suppressed APD alternans and whether decreasing I_{Kr} had the opposite effect.

Materials and Methods

This investigation conformed to the Guidelines for the Care and Use of Laboratory Animals published by the US National Institutes of Health (NIH publication no. 85-23). Experiments were approved by the Institutional Animal Care and Use Committee of the Center for Research Animal Resources at Cornell University. All animals used in these experiments were obtained from a colony of dogs maintained by Cornell University.

Microelectrode Recordings

Adult beagle dogs of either sex were anesthetized with Fatal-Plus (86 mg/kg IV), and their hearts were excised and placed in aerated (95% O_2 /5% CO_2) Tyrode solution containing (in mmol/L) NaCl 124, KCl 4.0, $NaHCO_3$ 24, NaH_2PO_4 0.9, $CaCl_2$ 2.0, $MgCl_2$ 0.7, and glucose 5.5; pH 7.4. Sections of left ventricular endocardial tissue measuring 2 cm \times 1 cm \times 2 mm were mounted in a Plexiglas chamber and superfused with Tyrode solution at 37°C. Transmembrane action potentials at different pacing CLs were recorded using standard microelectrode techniques. The recordings were sampled at 5 kHz and analyzed using programs written in Matlab 4.2c.

Isolation of Cardiac Myocytes

Endocardial myocytes were isolated by enzymatic dissociation as previously described.¹⁹ Briefly, a section of the ventricular free wall

supplied by the left circumflex coronary artery was perfused with Tyrode solution at 37°C for 10 to 15 minutes. Perfusion was then switched to Ca^{2+} -free perfusion solution containing (in mmol/L) NaCl 118, glucose 11, taurine 10, $NaHCO_3$ 25, KCl 4.8, mannitol 2, $MgSO_4$ 1.2, KH_2PO_4 1.2, glutamine 0.68, and pyruvate 5; adjusted to pH 7.3 with NaOH. After 3 to 5 minutes, the solution was switched to Ca^{2+} -free perfusion solution supplemented with collagenase (0.4 mg/mL) and BSA (0.5 mg/mL) for another 10 to 15 minutes. Thin slices of tissue were then dissected from the endocardium, minced, and agitated with 95% O_2 /5% CO_2 . After digestion, the supernatant was removed and replaced with perfusion solution to which HEPES (5 mmol/L) and $CaCl_2$ (1.0 mmol/L) had been added. The myocytes were studied during superfusion with extracellular solution containing (in mmol/L) NaCl 132, KCl 4, $MgCl_2$ 1, $CaCl_2$ 2, glucose 10, and HEPES 20; pH 7.4 at 37 \pm 1°C.

Action Potential Clamp Recordings

The perforated-patch voltage-clamp technique was used to minimize alterations of the intracellular milieu. Pipette solution contained (in mmol/L) aspartic acid 130, KCl 15, HEPES 10, $MgCl_2$ 2, and $CaCl_2$ 0.5; adjusted to pH 7.1 with KOH. Amphotericin B (0.21 mg/mL) was used as the pore-forming agent. The pipette tip resistance was 1 to 3 M Ω . Currents were low-pass filtered at 2 kHz and sampled at 5.5 kHz. The series resistance was approximately 20 M Ω , but was not compensated because the maximum current never exceeded 150 pA, and the corresponding voltage error was less than 3 mV. Data acquisition and analysis were performed using pClamp 8 (Axon Instruments, Inc).

Representative action potentials recorded at CLs of 1000, 500, 320, 170, and 120 ms were applied to the myocytes as the command potentials (Figure 1). Each action potential was applied six times, or in the case of alternans, six pairs of long and short action potentials were applied. I_{Kr} was defined as the drug-sensitive current blocked by E-4031 (5 μ mol/L; Wako). Baseline I_{Kr} was defined as the

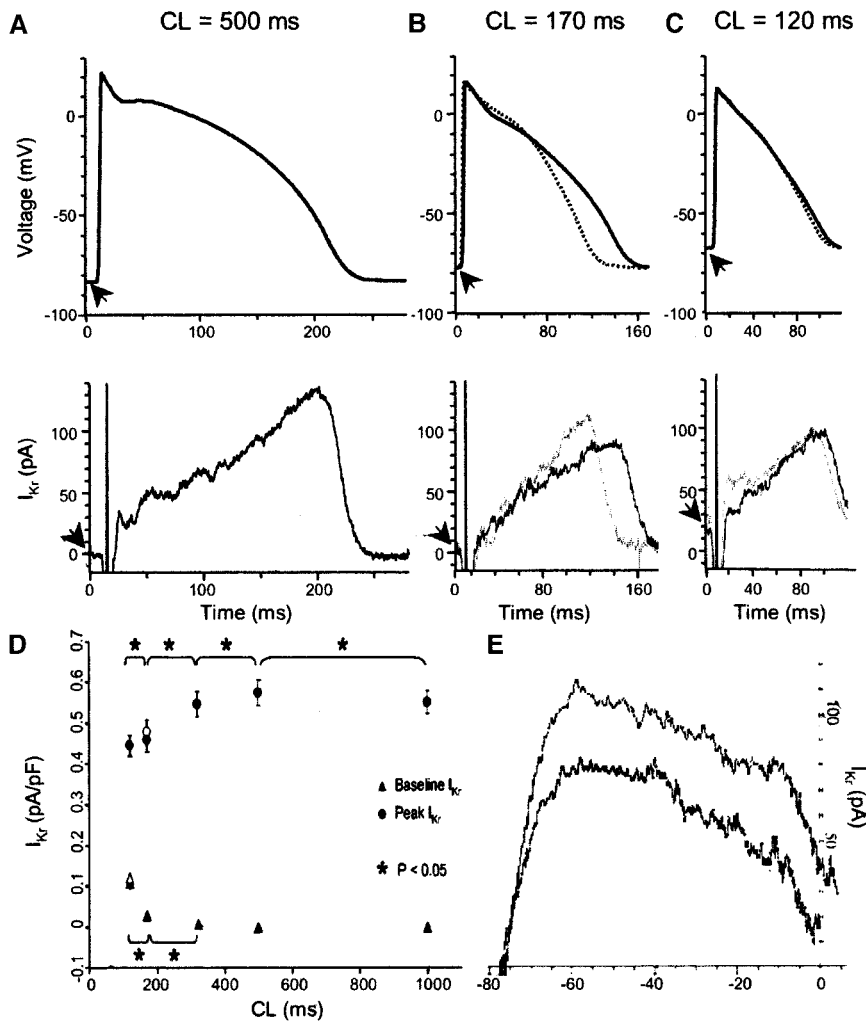


Figure 2. Rate-dependent alterations of I_{Kr} . Representative current traces measured as E-4031-sensitive currents (bottom) during action potentials (top) at CL=500 (A), 170 (B), and 120 ms (C). At CL=170 and 120 ms, solid and dotted lines represent the long and short action potentials, respectively, and their corresponding currents. Arrows indicate resting membrane potentials in the top and baseline I_{Kr} in the bottom. D, Summary of the relationship between peak I_{Kr} (circle), baseline I_{Kr} (triangle), and CL. During alternans at CL=170 and 120 ms, filled and unfilled symbols indicate values during the long and the short action potentials, respectively. * $P < 0.05$. E, Current plotted versus voltage for the long and short action potentials during pacing at CL=170 ms. Note that current during the short action potential (top trace) was greater for any given membrane potential than for the long action potential (bottom trace), reflecting increased g_{Kr} during the short action potential.

subtraction current immediately preceding the upstroke of the action potential. Peak I_{Kr} was defined as the absolute amplitude of the maximal subtraction current during repolarization. Conductance (g_{Kr}) was calculated according to $g = I/V$, where V is the membrane potential at which the current recording was obtained (V_m) minus the reversal potential for I_{Kr} (V_K), where $V_K = -86.1$ mV. Nisoldipine (2 μ mol/L) was present in the extracellular solutions to block L-type Ca^{2+} current for all recordings.

Statistical Analysis

All data are presented as mean \pm SE. Means were compared using paired Student's t test or 2-way ANOVA, followed by a Scheffe's F test, where appropriate. A value of $P < 0.05$ was considered significant.

Results

Rate-Dependent Alterations of I_{Kr}

Figure 2 shows representative recordings of I_{Kr} at different CLs and a summary of the mean data ($n = 20$). Peak I_{Kr} occurred during terminal repolarization at all CLs. Peak I_{Kr} density increased slightly, but significantly, from 0.55 ± 0.03 to 0.58 ± 0.03 pA/pF, as CL was reduced from 1000 to 500 ms. As CL was reduced further, peak I_{Kr} decreased progressively (Figure 2D). The membrane potentials at which peak I_{Kr} occurred were the same for CLs of 1000 ms (-55.6 ± 1.1 mV) and 500 ms (-55.5 ± 1.0 mV) and became slightly more

negative at a CL of 320 ms (-56.1 ± 1.1). During alternans at CLs of 170 and 120 ms, the membrane potentials at which peak I_{Kr} occurred were significantly more negative for the short action potentials than for the long action potentials (-58.9 ± 1.0 versus -57.0 ± 1.0 mV and -58.3 ± 1.0 versus -57.7 ± 1.0 mV, respectively).

During APD alternans at a CL of 170 ms, I_{Kr} increased at a slower rate and reached its maximum value at a later time during the long action potential than during the short action potential (Figure 2B). The peak magnitude of I_{Kr} was significantly less during the long action potential than during the short action potential (0.46 ± 0.03 versus 0.48 ± 0.03 pA/pF, respectively), as was the peak conductance (g_{Kr}) (15.8 ± 1.2 versus 17.6 ± 1.4 pS/pF, respectively) (Figure 2E). At a CL of 120 ms, the amplitude of APD alternans was reduced and the difference in peak I_{Kr} density between the long and short action potentials was no longer statistically significant (Figure 2C). Similarly, there were no significant differences in g_{Kr} between the long and short action potentials (15.7 ± 1.2 versus 16.0 ± 1.3 pS/pF, respectively).

Baseline I_{Kr} increased significantly at CLs of 170 and 120 ms (Figure 2D). There was no difference between baseline I_{Kr} during the long and short action potentials at a CL of 170 ms, whereas at a CL of 120 ms baseline I_{Kr} was significantly

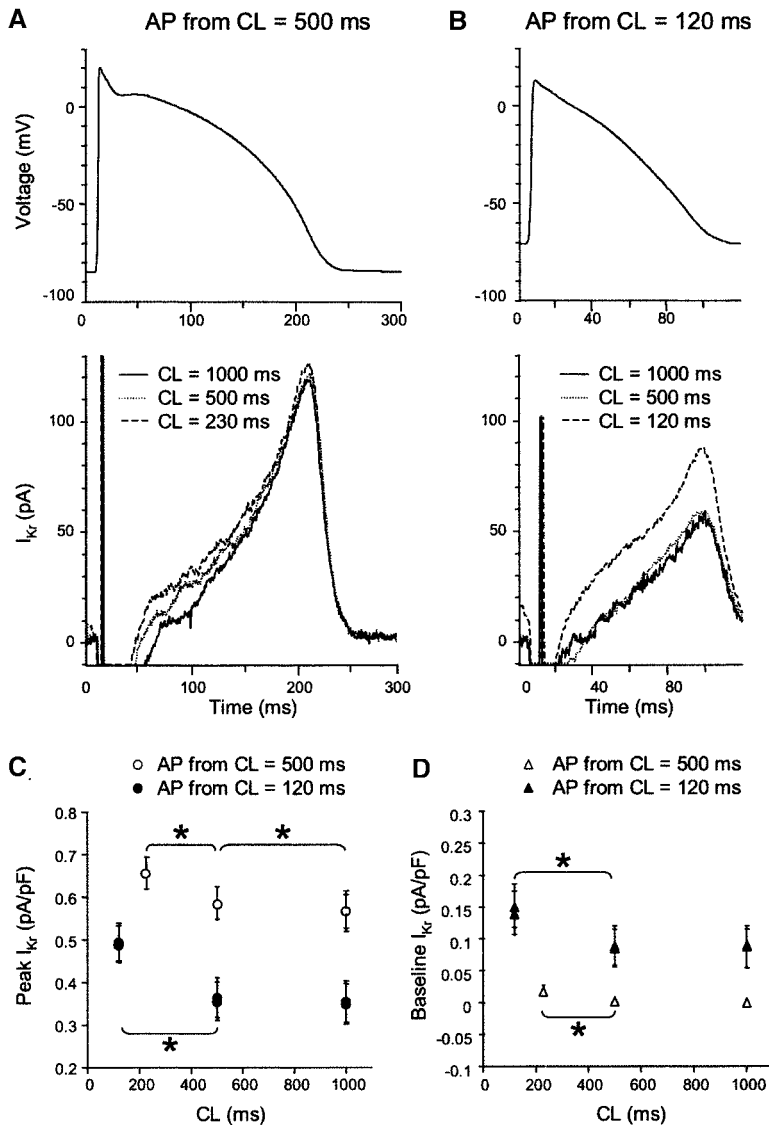


Figure 3. Rate-dependent accumulation of I_{Kr} . A, Action potential (AP) recorded at CL=500 ms (top) was applied at different CLs for action potential clamp. Bottom, Superimposed I_{Kr} at CL=1000 (solid line), 500 (dotted line), and 230 ms (broken line). B, Action potential recorded at CL=120 ms (top) was applied at different CLs for action potential clamp. Bottom, Superimposed I_{Kr} at CL=1000 (solid line), 500 (dotted line), and 120 ms (broken line). For clarity, only current traces during the long action potentials are shown. I_{Kr} during the short action potentials was similar. C, Summary of the relationship between peak I_{Kr} and CL for action potentials originally recorded at CL=500 ms (unfilled circle) and CL=120 ms (filled circle). D, Summary of the relationship between baseline I_{Kr} and CL for action potentials originally recorded at CL=500 ms (open triangle) and CL=120 ms (filled triangle). * $P < 0.05$.

smaller preceding the long action potential than the short action potential. The increase in baseline I_{Kr} at short CL may have been caused, in part, by the increased driving force resulting from depolarization of the resting membrane potential (from -85.0 mV at CL=1000 ms to -77.6 mV at CL=170 ms and to -71.1 mV at CL=120 ms). However, the increase in baseline I_{Kr} also was associated with an increase in g_{Kr} ($g_{Kr} = 0.14 \pm 0.01$ pS/pF at CL=1000 ms; 0.15 ± 0.01 pS/pF at CL=500 ms; 2.2 ± 0.15 pS/pF at CL=320 ms; 3.1 ± 0.22 and 3.4 ± 0.23 pS/pF for the long and short action potentials, respectively, at CL=170 ms; 7.2 ± 0.64 and 8.0 ± 0.68 pS/pF for the long and short action potentials, respectively, at CL=120 ms). The difference in g_{Kr} between the long and short action potentials was statistically significant at a CL of 120 ms, but not at 170 ms.

Rate-Dependent Accumulation of I_{Kr}

In the experiments described, the CLs were varied and the shape of the action potential at each CL also differed. To isolate the effect of CL on I_{Kr} , a single action potential waveform was applied at different CLs (Figure 3). The action potential recorded

at a CL of 500 ms (Figure 3A) was applied at CLs of 1000, 500, and 230 ms to 23 myocytes. Because APD at 90% repolarization (APD₉₀) at a CL of 500 ms was 214 ms, the shortest CL that could be delivered without encroaching on the action potential was 230 ms. As shown in Figure 3, peak I_{Kr} increased as CL was shortened, whereas baseline I_{Kr} did not differ between CL of 1000 ms and 500 ms, but increased slightly at a CL of 230 ms. The membrane potential at which peak I_{Kr} occurred was similar for all three CLs.

The action potentials recorded at a CL of 120 ms (Figure 3B) were applied at CLs of 1000, 500, and 120 ms to 12 myocytes. Peak I_{Kr} was similar at CLs of 1000 and 500 ms, but increased at a CL of 120 ms (Figures 3B and 3C). There was no difference in peak I_{Kr} between the long and short action potentials at any CL. Baseline I_{Kr} was similar at CLs of 1000 and 500 ms and was not different between the long and short action potentials at these CLs. However, baseline I_{Kr} increased at a CL of 120 ms and was smaller preceding the long action potential than the short action potential. The membrane potential at which peak I_{Kr} occurred was similar, regardless of CL.

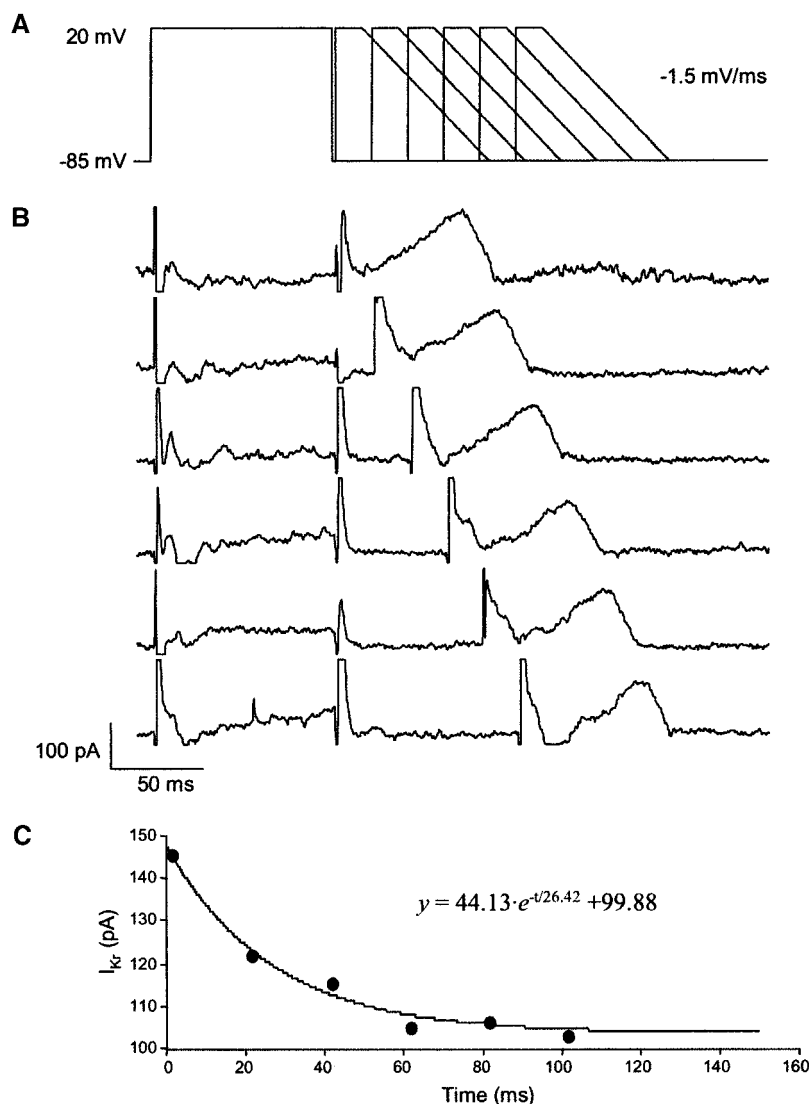


Figure 4. Time constant of deactivation of I_{Kr} at -85 mV. A, Voltage-clamp protocol. B, Representative current traces. Sweeps were separated for clarity. Peak I_{Kr} during the repolarizing ramp decreased with a longer delay before the second pulse. C, Relationship between peak I_{Kr} and the time interval between 2 pulses was fit to a single exponential equation with a time constant of 26 ms.

Time Constant for Deactivation

To determine whether the increase in baseline I_{Kr} at short CL was caused by slow deactivation of the current, the time course of deactivation was measured using a double-pulse protocol (Figure 4). The initial pulse was stepped to $+20$ mV for 100 ms from a holding potential of -85 mV and then back to either -85 , -70 , or -55 mV, depending on the voltage at which the time constant was to be measured. The second pulse was a square-ramp pulse (to simulate the shape of an action potential) with a 15-ms square pulse to $+20$ mV followed by a ramp from $+20$ mV to -85 mV over 70 ms. Peak current was measured during the repolarization ramp. The interpulse interval was 2 ms initially and increased by 20 ms for measuring the time constant at -85 mV and by 50 ms for measuring the time constants at -70 and -55 mV.

Figure 4B shows a representative recording used to determine the deactivation time constant at -85 mV. The current elicited by the square-ramp pulse was similar to I_{Kr} recorded during action potential clamp. The relationship between the peak current amplitude and the interpulse interval was fit by a single exponential equation. The mean time constants for

deactivation at -85 , -70 , and -55 mV were 34.0 ± 6.3 ms ($n=7$), 48.8 ± 7.0 ms ($n=7$), and 116.4 ± 7.6 ms ($n=6$), respectively.

Computer Simulation

A computer model for I_{Kr} was developed on the basis of the Winslow model²⁰ and our subsequent modification of the Winslow model for the canine ventricular myocyte (CVM).¹⁰ The model was driven by the same action potentials used for the voltage clamp experiments. To fit the experimental data, the parameters for I_{Kr} used in the CVM model were modified as follows: the voltage-dependence of steady-state activation was shifted to less negative membrane potentials; the time constant for deactivation was markedly reduced; the voltage-dependence of steady-state inactivation was flattened and was shifted to more negative membrane potentials; a time constant for inactivation was introduced and; maximum conductance was increased (Figures 5A through 5D) (also see Appendix). Thus modified, the model generated a current that faithfully reproduced the I_{Kr} recorded experimentally (Figures 5E through 5F).

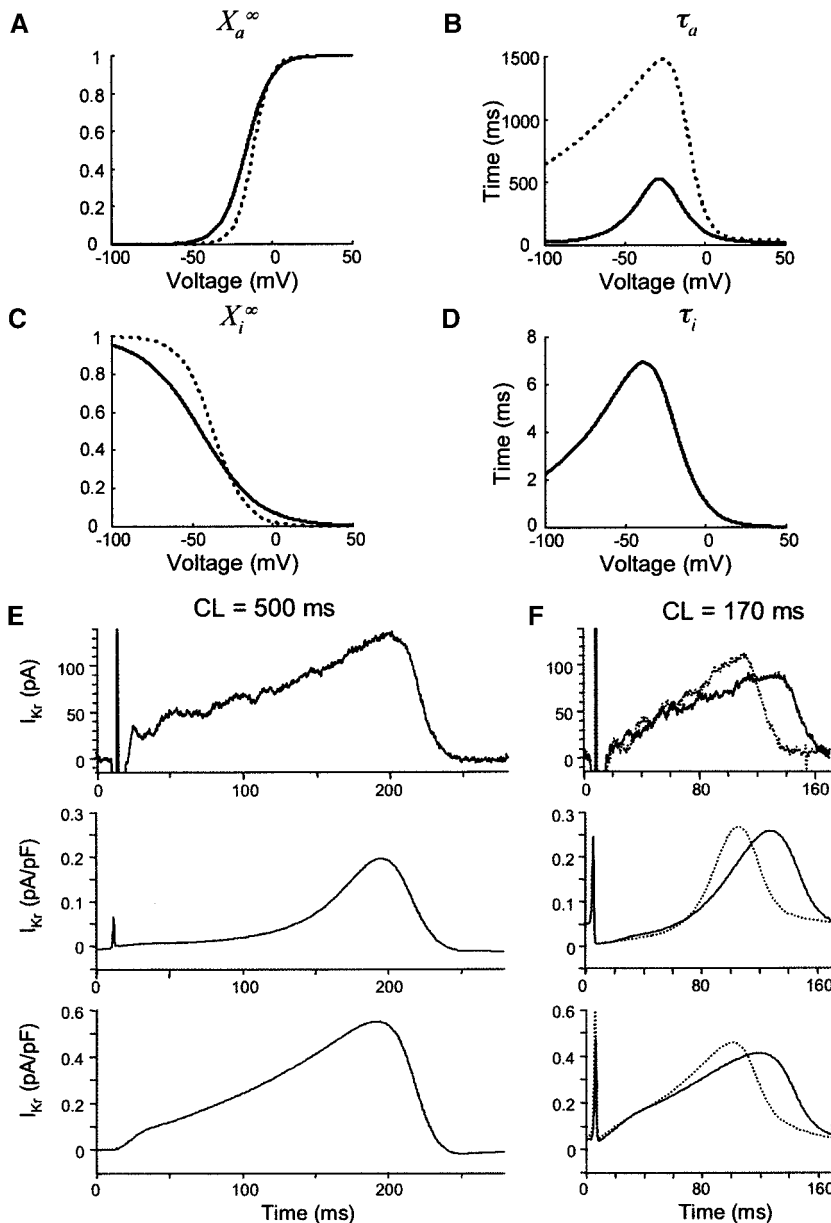


Figure 5. Computer model for I_{Kr} . A through D, Parameters used in the model: voltage-dependent steady-state activation curve (A), voltage-dependent time constant for activation and deactivation (B), voltage-dependent steady-state inactivation curve (C), and voltage-dependent time constant for inactivation and recovery from inactivation (D). Solid and dotted lines are the parameters used in the modified I_{Kr} model and the CVM model. E and F, I_{Kr} during action potentials (as in Figure 2) at CL=500 (E) and 170 ms (F) generated by the computer simulation using the CVM model (middle) and the modified I_{Kr} model (bottom) compared with experimental data (top). At CL=170 ms, the solid and dotted lines represent current traces during the long and short action potentials, respectively.

The modified I_{Kr} model subsequently was used to study the mechanism for alternating peak I_{Kr} during APD alternans at CL=170 ms. Figure 6 shows changes in the open probability of the activation (X_a) and inactivation (X_i) gates. The open probability of the inactivation gate (X_i) did not vary significantly from beat to beat and followed the shape of the action potential, as expected from its fast kinetics. In contrast, the open probability of the activation gate (X_a) exhibited large beat-to-beat variations. During the long action potential, there was insufficient time for the activation gate to close completely (ie, open probability did not return to zero), which resulted in a fraction of channels remaining open before the next action potential. Consequently, X_a for the next (short) action potential was larger. In addition, the more positive plateau voltage during the short action potential activated more channels than during the long action potential. Together, incomplete deactivation at the end of the long action

potential and a higher plateau during the short action potential produced a larger peak I_{Kr} during the short action potential.

The CVM model incorporated with modified I_{Kr} also was used to test whether increasing I_{Kr} suppressed APD alternans. I_{Kr} was increased by (1) increasing conductance, (2) shifting the voltage-dependence of steady-state activation to more negative membrane potentials, (3) shifting the voltage-dependence of steady-state inactivation to less negative membrane potentials, and (4) increasing the time constant for deactivation (Figure 7A). Each of these alterations abolished APD alternans (Figure 7B), in association with minimal changes in the APD restitution relation (Figure 7D). After increasing I_{Kr} , peak L-type Ca^{2+} current (I_{Ca}) increased slightly during pacing at a CL of 400 ms (from 1.6 to 1.7 pA/pF), and the normal alternation of I_{Ca} during pacing at a CL of 160 (between 1.4 and 1.0 pA/pF) was suppressed (I_{Ca} was constant at 1.1 pA/pF).

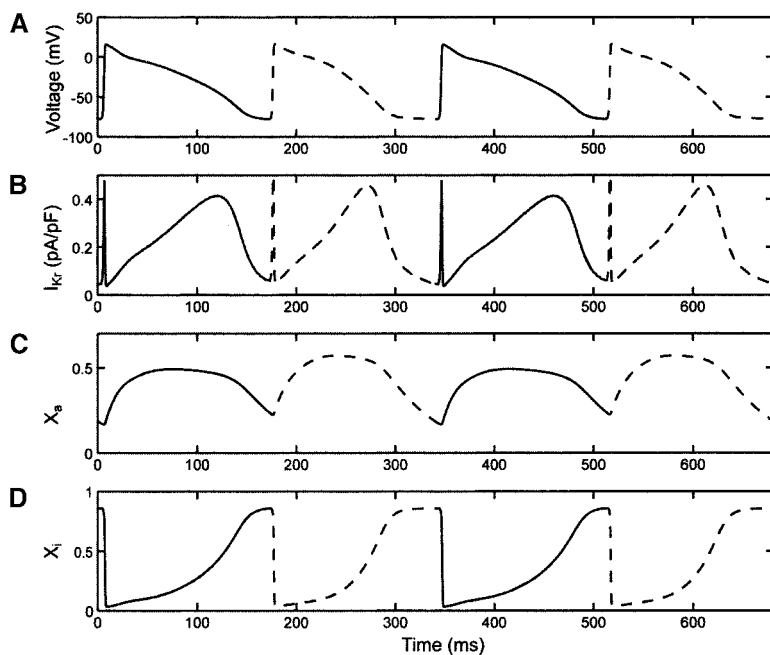


Figure 6. Mechanisms for alterations of peak I_{Kr} during APD alternans (computer simulation). A, Long (solid line) and short (broken line) action potentials at CL=170 ms. B, I_{Kr} during action potentials. Peak I_{Kr} was larger during the short action potential (broken line) than during the long action potential (solid line). C, Open probability of the activation gate (X_s) during action potentials. D, Open probability of the inactivation gate (X_i) during action potentials.

We also tested whether decreasing I_{Kr} increased the magnitude of APD alternans in the modified model, as was shown previously in the original CVM model.¹⁰ As I_{Kr} was decreased progressively by reducing maximal conductance, APD increased, and the magnitude of APD alternans increased as well. Figure 7C shows an example of the effects of decreasing I_{Kr} conductance from 0.0541 to 0.0441 mS/ μ F on steady-state APD and the magnitude of APD alternans. In this particular case, the magnitude of APD alternans was increased despite a small reduction in the slope of the dynamic APD restitution relation (from 1.170 to 1.147) (Figure 7D).

Effect of Blocking I_{Kr} on Action Potential Dynamics

The prediction that decreasing I_{Kr} increases the magnitude of APD alternans was tested by evaluating the effects of the I_{Kr} antagonist E-4031 on rate-dependent changes of APD. The effects of E-4031 on action potential morphology of endocardial tissue ($n=5$) at a CL of 400 and 120 ms are shown in Figure 8. E-4031 had minimal effect on the plateau phase of the action potential, but markedly prolonged terminal repolarization. At the longer CL, both APD₉₀ and APD₅₀ were significantly prolonged by E-4031. At a CL of 120 ms, E-4031 did not alter APD₅₀ for either the long or the short action potential (Figure 8B). However, E-4031 significantly prolonged APD₉₀ of the short action potential (from 88.8 ± 1.7 to 96.5 ± 3.0 ms) and tended to prolong APD₉₀ of the long action potential (from 99.8 ± 2.0 to 105.5 ± 1.2 ms), but the latter effect was not statistically significant ($P=0.1$) (Figure 8B). The maximum amplitude of APD alternans was increased by approximately 50% in the presence of E-4031, from 13.5 ± 3.2 to 19.2 ± 2.4 ms for APD₉₀ (Figure 8C), in concert with an increase in the slope of the dynamic APD restitution relation from 1.2 ± 0.03 to 1.54 ± 0.07 . An example of the effects of E-4031 on the APD restitution relation is shown in Figure 8D.

Discussion

Inherited or drug-induced abnormalities of I_{Kr} have been linked to a variety of cardiac arrhythmias,^{17,21,22} most of which are thought to be precipitated by bradycardia-induced prolongation of repolarization. The potential mechanisms by which I_{Kr} may facilitate the induction of arrhythmias at slow heart rates have been studied extensively.^{12,23,24} However, the contribution of I_{Kr} to repolarization during tachycardia, which might also be important for the development of cardiac arrhythmias, has not been well characterized. In this study, we measured I_{Kr} during action potentials elicited by pacing at normal to high frequencies. The results indicate that the magnitude of I_{Kr} is determined by multiple factors, including (1) the membrane potential during the action potential plateau, (2) the duration of the plateau, (3) the membrane potential during the diastolic interval, and (4) the duration of the diastolic interval. Interactions between these factors are complex, precluding straightforward relationships between stimulation rate, APD, and I_{Kr} amplitude. In general, peak I_{Kr} amplitude is smaller at faster stimulation rates, yet during APD alternans I_{Kr} is larger during the shorter action potential than during the longer action potential.

Rate-Dependent Alterations of I_{Kr}

As CL was decreased progressively, peak I_{Kr} increased initially and then decreased (Figure 2). The mechanism for the small initial increase of peak I_{Kr} is unclear, given that action potential morphology for CLs of 1000 and 500 ms was the same. On the other hand, the more marked reduction of peak I_{Kr} at short CL appeared to be caused by decreased channel activation, secondary to the shorter action potential plateau duration and a less positive membrane potential during the plateau.

During progressive reduction of CL, baseline I_{Kr} during the diastolic interval remained constant before increasing at the shortest CLs. The increase in baseline I_{Kr} was associated with

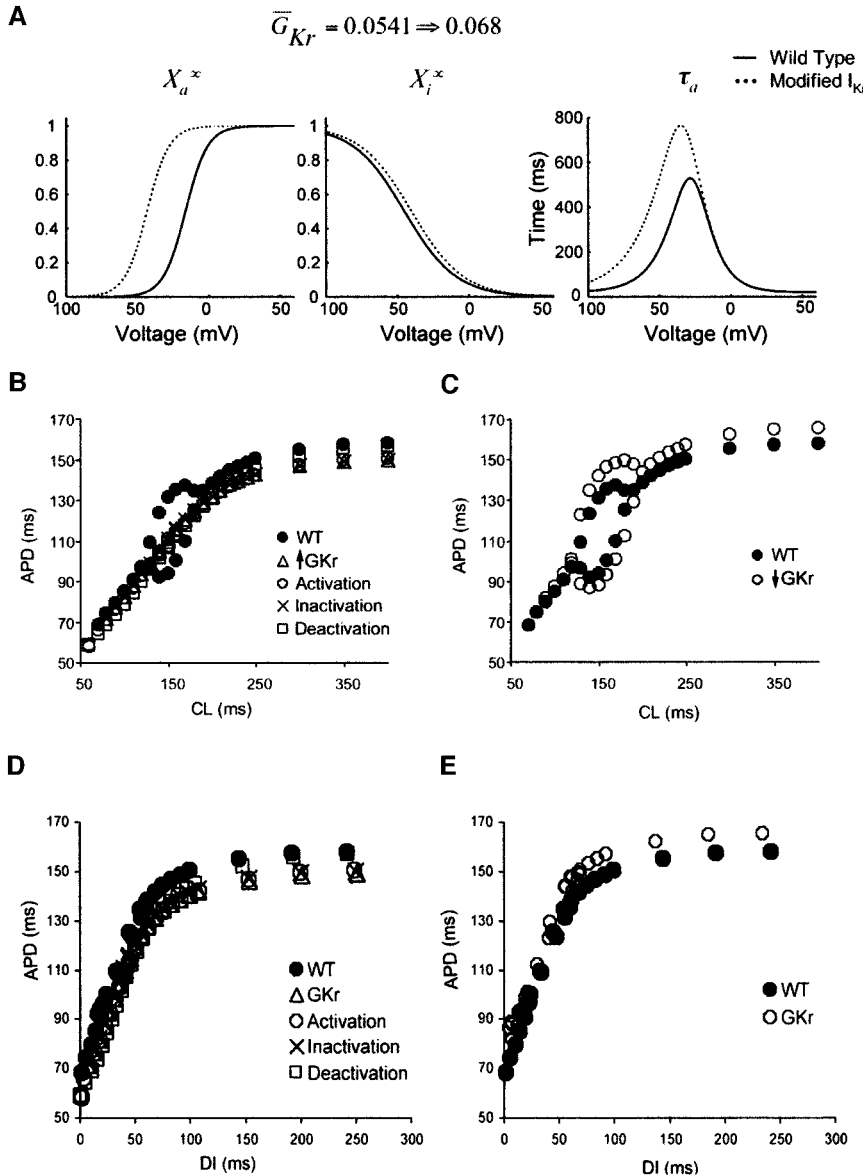


Figure 7. Computer simulation of the effects of increasing I_{Kr} by altering channel kinetics or conductance on APD alternans. **A**, Modifications of the model used to increase I_{Kr} . Top, Increasing conductance (G_{Kr}). Bottom, From left to right, shifting the steady-state activation curve to the left; shifting the steady-state inactivation curve to the right; increasing the time constant of deactivation. **B**, Relationship between APD and CL generated by CVM models with wild-type I_{Kr} (filled circle) and increased I_{Kr} (see legend). For wild-type I_{Kr} , there were 2 values of APD for one CL during APD alternans. **C**, Relationship between APD and CL generated by models with wild-type I_{Kr} (filled circle) and decreased I_{Kr} produced by decreasing conductance (open circle). **D** and **E**, Relationships between APD and DI corresponding to the plots shown in **B** and **C**, respectively.

depolarization of the resting membrane potential. Although I_{Kr} did not activate at membrane potentials more negative than -60 mV (Figure 5A), significant I_{Kr} was detected at -71.1 mV (the resting potential for CL=120 ms). The presence of I_{Kr} at this membrane potential can be attributed to incomplete deactivation, secondary to the slow time course of deactivation and the short diastolic intervals that occur at short CLs.

Slow deactivation is one of the most prominent characteristics of I_{Kr} , both in the dog^{25,32} and in other species.^{26,27,33} However, in previous studies, the deactivation kinetics of I_{Kr} was evaluated at membrane potentials less than -60 mV, primarily because at more negative voltages the amplitude of the current is small, secondary to a reduced driving force near the reversal potential. In our study, a two-pulse protocol was used to elicit larger currents, which enabled us to measure the deactivation time constant at more negative potentials. Those measurements indicated that the deactivation time constants of I_{Kr} at -85 and -70 mV were on the order of 35 to 50 ms, which were sufficiently slow to prevent complete deactivation

during pacing at short CLs. The primary manifestation of incomplete deactivation was increased baseline I_{Kr} during pacing at short CLs. The presence of significant I_{Kr} during the diastolic interval suggests that I_{Kr} may help to offset the depolarization of resting membrane potential that typically occurs during rapid pacing.

I_{Kr} During APD Alternans

During APD alternans at a CL of 170 ms, peak I_{Kr} was larger during the shorter action potential, in part because the plateau voltage during the short action potential was more positive than during the long action potential, resulting in activation of more I_{Kr} . In addition, the rate of repolarization was faster for the shorter action potential, which provided less time for the channel to deactivate. Finally, the short action potential was preceded by a short diastolic interval, during which deactivation of I_{Kr} may have been incomplete, resulting in a fraction of channels being activated before the onset of the short action potential. However, the contribution of baseline I_{Kr} to

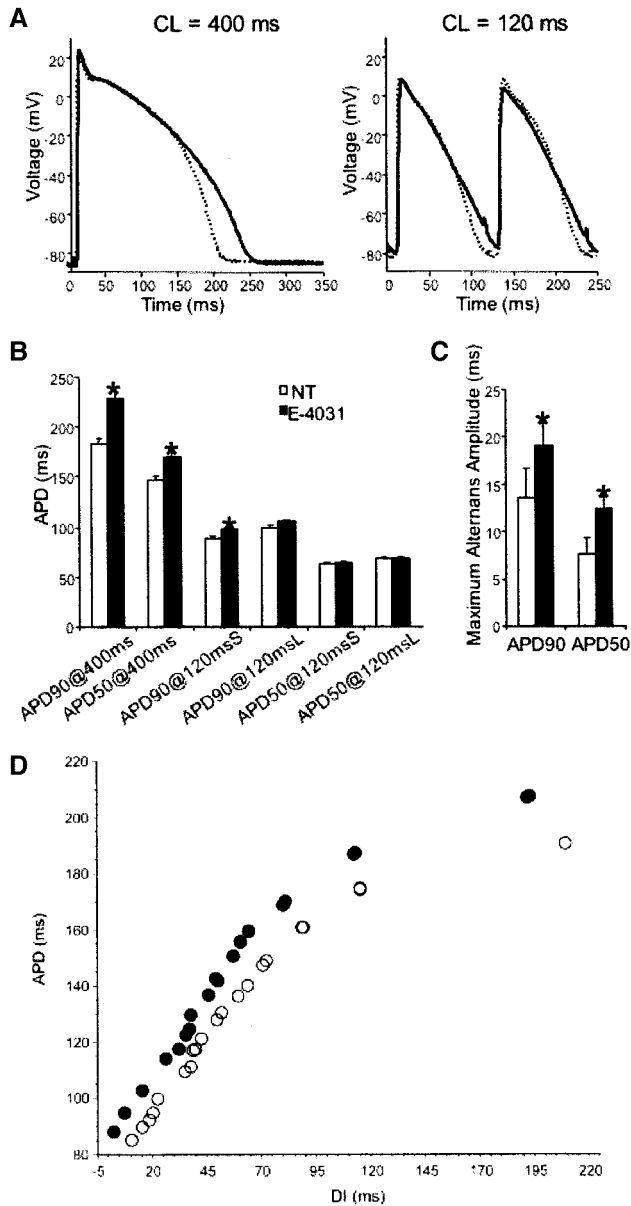


Figure 8. Effects of E-4031 on action potential dynamics. A, Action potentials before (dotted line) and after (solid line) exposure to E-4031 (5 μ mol/L) at CL=400 and 120 ms. B, Effects of E-4031 on APD₉₀ and APD₅₀ at CL=400 ms and on long and short action potentials at CL=120 ms. C, Effects of E-4031 on the maximum alternans amplitude for APD₉₀ and APD₅₀. **P*<0.05. D, Example of APD restitution relations before (open symbols) and after (filled symbols) exposure to E-4031.

the peak current apparently was small, given that at a CL of 120 ms, baseline current was greater than at a CL of 170 ms, yet peak I_{Kr} was smaller.

Potential Implications

Decreasing I_{Kr} , both in the computer model and pharmacologically, increased the magnitude of APD alternans. Conversely, increasing I_{Kr} in the computer model, either by increasing channel conductance or by altering channel kinetics, suppressed alternans. Given that APD alternans has been linked to the development of ventricular fibrillation,^{6,8,28,29}

modifications of I_{Kr} might be expected to alter the risk of sudden death. In that regard, the results of this study may provide at least a partial explanation for the proarrhythmic effects of certain I_{Kr} blockers¹²⁻¹⁶ and a rationale for the development of a new class of putative antiarrhythmic agents, I_{Kr} agonists.

Questions remain, however, regarding whether augmentation of I_{Kr} or other K currents selectively reduces APD alternans magnitude or whether the effects of such drugs relate to a nonspecific shortening of APD.^{10,30} Recent theoretical studies have suggested that K current, I_{Kr} in particular, may contribute to so-called cardiac memory, as it exists on a beat-to-beat time scale.³¹ Modest increases in I_{Kr} eliminate APD alternans with little or no attendant shortening of APD and tend to increase, rather than flatten, the slope of the APD restitution relation.^{10,31} These observations suggest that titration of K channel agonism may produce a selective inhibition of alternans. Unfortunately, tests of this idea must await the development of a selective I_{Kr} agonist, as none currently exists.

Appendix

I_{Kr} in the CVM model was modified to fit the experimental data. The formulations and parameters for modified I_{Kr} are as follows:

$$I_{Kr} = \overline{G_{Kr}} X_{Kr} Y_{Kr} \sqrt{[K^+]_o} / 4 (V - E_{Kr})$$

$$\frac{dX_{Kr}}{dt} = \frac{X_{Kr}^\infty - X_{Kr}}{\tau X_{Kr}}$$

$$\frac{dY_{Kr}}{dt} = \frac{Y_{Kr}^\infty - Y_{Kr}}{\tau Y_{Kr}}$$

$$X_{Kr}^\infty = \frac{1}{1 + e^{-(v+16.5)/7.8}}$$

$$\tau X_{Kr} = 20.0 + \frac{1}{e^{-4.5+0.09V} + e^{-8.8-0.07V}}$$

$$Y_{Kr}^\infty = \frac{1}{1 + e^{(v+45.0)/18}}$$

$$\tau Y_{Kr} = \frac{1}{e^{-0.1+0.09V} + e^{-3.0-0.022V}}$$

$$\overline{G_{Kr}} = 0.0541 \text{ mS}/\mu\text{F}$$

where X_{Kr} and Y_{Kr} are the time- and voltage-dependent open probabilities of activation and inactivation gates, G_{Kr} is the maximum conductance of I_{Kr} , V is the membrane potential, and $E_{Kr} = -85$ mV is the reversal potential of I_{Kr} channel with physiological ionic concentrations both inside and outside the cell. X_{Kr}^∞ and Y_{Kr}^∞ are the steady-state voltage-dependent open probabilities of the activation and inactivation gates; τX_{Kr} and τY_{Kr} are the voltage-dependent activation and inactivation time constants.

To obtain the same amplitude of APD alternans as in the original CVM model, P_{Kr} was increased to 0.000028 cm/ms. All of the other equations and parameters were unchanged from the original CVM model.

Acknowledgments

These studies were supported by a predoctoral fellowship from the American Heart Association, New York State Affiliate, Inc, and NIH grant HL 62543. We thank Dr Jeffrey J. Fox for advice regarding the

computer model, Dr Andrew Zygmunt for assistance with the perforated patch-clamp technique, and Dr Lisa C. Freeman for a critical and constructive review of the manuscript.

References

- Saitoh H, Bailey JC, Surawicz B. Alternans of action potential duration after abrupt shortening of cycle length: differences between dog Purkinje and ventricular muscle fibers. *Circ Res*. 1988;62:1027–1040.
- Koller ML, Riccio ML, Gilmour RF Jr. Dynamic restitution of action potential duration during electrical alternans and ventricular fibrillation. *Am J Physiol*. 1998;275:H1635–H1642.
- Koller ML, Riccio ML, Gilmour RF Jr. Effects of $[K^+]_o$ on electrical restitution and activation dynamics during ventricular fibrillation. *Am J Physiol Heart Circ Physiol*. 2000;279:H2665–H2672.
- Riccio ML, Koller ML, Gilmour RF Jr. Electrical restitution and spatio-temporal organization during ventricular fibrillation. *Circ Res*. 1999;84:955–963.
- Boyett MR, Jewell BR. Analysis of the effects of changes in rate and rhythm upon electrical activity in the heart. *Prog Biophys Mol Biol*. 1980;36:1–52.
- Chialvo DR, Michaels DC, Jalife J. Supernormal excitability as a mechanism of chaotic dynamics of activation in cardiac Purkinje fibers. *Circ Res*. 1990;66:525–545.
- Chialvo DR, Gilmour RF Jr, Jalife J. Low dimensional chaos in cardiac tissue. *Nature*. 1990;343:653–657.
- Guevara MR, Ward R, Shrier A, Glass L. Electrical alternans and period doubling bifurcations. *IEEE Comp Cardiol*. 1984;167–170.
- Boyett MR, Jewell BR. A study of the factors responsible for rate-dependent shortening of the action potential in mammalian ventricular muscle. *J Physiol*. 1978;285:359–380.
- Fox JJ, McHarg JL, Gilmour RF Jr. Ionic mechanism of electrical alternans. *Am J Physiol Heart Circ Physiol*. 2002;282:H516–H530.
- Choi BR, Salama G. Simultaneous maps of optical action potentials and calcium transients in guinea-pig hearts: mechanisms underlying concordant alternans. *J Physiol*. 2000;529:171–188.
- Jurkiewicz NK, Sanguinetti MC. Rate-dependent prolongation of cardiac action potentials by a methanesulfonanilide class III antiarrhythmic agent: specific block of rapidly activating delayed rectifier K^+ current by dofetilide. *Circ Res*. 1993;72:75–83.
- Waldo AL, Camm AJ, deRuyter H, Friedman PL, MacNeil DJ, Pauls JF, Pitt B, Pratt CM, Schwartz PJ, Veltri EP. Effect of D-sotalol on mortality in patients with left ventricular dysfunction after recent and remote myocardial infarction. The SWORD Investigators. Survival With Oral D-Sotalol. *Lancet*. 1996;348:7–12.
- Keating MT, Sanguinetti MC. Molecular genetic insights into cardiovascular disease. *Science*. 1996;272:681–685.
- Mohammad S, Zhou Z, Gong Q, January CT. Blockage of the HERG human cardiac K^+ channel by the gastrointestinal prokinetic agent cisapride. *Am J Physiol*. 1997;273:H2534–H2538.
- Roy M, Dumaine R, Brown AM. HERG, a primary human ventricular target of the non-sedating antihistamine terfenadine. *Circulation*. 1996;94:817–823.
- Curran ME, Splawski I, Timothy KW, Vincent GM, Green ED, Keating MT. A molecular basis for cardiac arrhythmia: HERG mutations cause long QT syndrome. *Cell*. 1995;80:795–803.
- Roden DM, Balse JR. A plethora of mechanisms in the HERG-related long QT syndrome: genetics meets electrophysiology. *Cardiovasc Res*. 1999;44:242–246.
- Paciorety LM, Gilmour RF Jr. Restoration of transient outward current by norepinephrine in cultured canine cardiac myocytes. *Am J Physiol*. 1998;275:H1599–H1605.
- Winslow RL, Rice J, Jafri S, Marban E, O'Rourke B. Mechanisms of altered excitation-contraction coupling in canine tachycardia-induced heart failure, II: model studies. *Circ Res*. 1999;84:571–586.
- Sanguinetti MC, Jiang C, Curran ME, Keating MT. A mechanistic link between an inherited and an acquired cardiac arrhythmia: HERG encodes the I_{Kr} potassium channel. *Cell*. 1995;81:299–307.
- Mitcheson JS, Chen J, Lin M, Culberson C, Sanguinetti MC. A structural basis for drug-induced long QT syndrome. *Proc Natl Acad Sci U S A*. 2000;97:12329–12333.
- Roden DM. Acquired long QT syndromes and the risk of proarrhythmia. *J Cardiovasc Electrophysiol*. 2000;11:938–940.
- Hondeghem LM, Snyders DJ. Class III antiarrhythmic agents have a lot of potential but a long way to go: reduced effectiveness and dangers of reverse use dependence. *Circulation*. 1990;81:686–690.
- Gintant GA. Regional differences in I_{Ks} density in canine left ventricle: role of I_{Ks} in electrical heterogeneity. *Am J Physiol*. 1995;268:H604–H613.
- Clay JR, Ogbaghebriel A, Paquette T, Sasnyuk BI, Shrier A. A quantitative description of the E-4031-sensitive repolarization current in rabbit ventricular myocytes. *Biophys J*. 1995;69:1830–1837.
- Follmer CH, Lodge NJ, Cullinan CA, Colatsky TJ. Modulation of the delayed rectifier, I_{Ks} , by cadmium in cat ventricular myocytes. *Am J Physiol*. 1992;262:C75–C83.
- Fox JJ, Riccio ML, Hua F, Bodenschatz E, Gilmour RF Jr. Spatio-temporal transition to conduction block in canine ventricle. *Circ Res*. 2002;90:289–296.
- Garfinkel A, Kim Y-H, Voroshilovsky O, Qu Z, Kil JR, Lee M-H, Karagueuzian HS, Weiss JN, Chen P-S. Preventing ventricular fibrillation by flattening cardiac restitution. *Proc Natl Acad Sci U S A*. 2000;97:6061–6066.
- Qu Z, Weiss JN, Garfinkel A. Cardiac electrical restitution properties and stability of reentrant spiral waves: a simulation study. *Am J Physiol*. 1999;276:H269–H283.
- Fox JJ, Riccio ML, Drury P, Werthman A, Gilmour RF Jr. Dynamic mechanism for conduction block in heart tissue. *New J Phys* 2003;5:101.1–101.14.
- Gintant GA. Characterization and functional consequences of delayed rectifier current transient in ventricular repolarization. *Am J Physiol Heart Circ Physiol*. 2000;278:H806–H817.
- Rocchetti M, Besana A, Gurrrola GB, Possani LD, Zaza A. Rate dependency of delayed rectifier currents during the guinea-pig ventricular action potential. *J Physiol*. 2001;534:721–732.